

# Supplementary material for NAM: Neural Adjoint Maps for refinement of shape correspondences

GIULIO VIGANÒ, University of Milano-Bicocca, Italy  
 MAKS OVSJANIKOV, LIX, Ecole Polytechnique, France  
 SIMONE MELZI, University of Milano-Bicocca, Italy

## ACM Reference Format:

Giulio Viganò, Maks Ovsjanikov, and Simone Melzi. 2025. Supplementary material for NAM: Neural Adjoint Maps for refinement of shape correspondences. *ACM Trans. Graph.* 1, 1 (June 2025), 4 pages. <https://doi.org/10.1145/nnnnnnnn.nnnnnnnn>

## 1 Supplementary

This document provides proofs, additional details, and results to complement the main text of the manuscript.

### 1.1 Proofs

In this Section, we prove the following propositions of the main manuscript.

**PROPOSITION 1.1.** *Given a function  $g : \mathbb{R}^k \rightarrow \mathbb{R}^k$  such that  $g(\Phi_1^k) = \Pi_{21}\Phi_2^k$ , then a NAM  $h$  realizes  $E_{NAM}(h) = 0$  in Equation (4.11) if and only if*

$$h \circ g = I_1 \quad (1)$$

where  $I_1$  is the identity function on  $\Phi_1^k$ .

**PROOF.** Applying  $g$  and then  $h$  to  $\Phi_1^k$  we obtain:  $h(g(\Phi_1^k)) = h(\Pi_{21}\Phi_2^k)$ . The action of  $h$  is defined row-wise, so we have  $h(\Pi_{21}\Phi_2^k) = \Pi_{21}h(\Phi_2^k)$ . Suppose that  $h$  realizes the 0 in Equation (4.11), then we can write  $\Pi_{21}h(\Phi_2^k) = \Phi_1^k$ , and thus  $h(g(\Phi_1^k)) = \Phi_1^k$  which provides the first part of the proof.

Now suppose that Equation (1) holds for a given  $h$ , which is  $h(g(\Phi_1^k)) = h(\Pi_{21}\Phi_2^k) = \Pi_{21}h(\Phi_2^k) = \Phi_1^k$ . Taking the last equivalence, we have that (11) is equal to 0 for this  $h$ , and this completes the proof.  $\square$

**PROPOSITION 1.2.**  $\Phi_1^k$  and  $\Phi_2^k$  are linearly alignable for any  $k \leq n$  iff the shapes are isometric.

**PROOF.** Isometric shapes imply that  $\Phi_1^k$  and  $\Phi_2^k$  are linearly alignable for any  $k \leq n$  is trivial.

The other direction can be proved by induction considering the orthonormality of the basis. For  $k = 1$ , we consider the two constant eigenfunctions. If they are alignable, then  $\phi_1^1 = a\phi_2^1$  where  $a$  is a constant. But the orthonormality of the shapes implies that  $a =$

Authors' Contact Information: Giulio Viganò, University of Milano-Bicocca, Italy, g.vigan36@campus.unimib.it; Maks Ovsjanikov, LIX, Ecole Polytechnique, France; Simone Melzi, University of Milano-Bicocca, Italy.



This work is licensed under a Creative Commons Attribution 4.0 International License.  
 © 2025 Copyright held by the owner/author(s).  
 ACM 1557-7368/2025/6-ART  
<https://doi.org/10.1145/nnnnnnnn.nnnnnnnn>

$\pm 1$ . If  $\Phi_1^k = \Phi_2^k A^k$  implies that  $\phi_1^i = \pm \phi_2^i$  for all  $i \in \{0, \dots, k\}$ , then  $A^k$  is a diagonal matrix of 1 and  $-1$  entries. Then if  $\Phi_1^{k+1} = \Phi_2^{k+1} A^{k+1}$ ,  $A[k+1, k+1] = \pm 1$ . If this does not hold, it means it exists at least one  $l \in \{0, \dots, k\}$  such that  $\phi_1^{k+1} = a_{k+1, k+1} \phi_2^{k+1} + a_{l, k+1} \phi_2^l$  but for the orthonormality of  $span(\{\phi_1^j\}_{j=0}^k)$  and  $\phi_1^{k+1}$  this is not possible. This proves that if the spectra embeddings are alignable in each dimension the shapes are isometric.  $\square$

### 1.2 Functional Maps

We report the rigorous derivation of the functional map. If we equip the functional spaces with bases  $\Phi_1$  and  $\Phi_2$ , we can represent each function as a vector of the coefficients of its representation in the basis, thus for each  $f \in \mathcal{X}_1, g \in \mathcal{X}_2$  there exist vector of coefficients  $\underline{a} = (a_i)$  and  $\underline{b} = (b_j)$  such that  $f = \sum_i a_i \phi_1^i = \phi_1 \underline{a}$  and  $g = \sum_j b_j \phi_2^j = \phi_2 \underline{b}$ . Thanks to this representation and the linearity of the functional map we have:

$$T_{21}^F(g) = T_{21}^F(\sum_j b_j \phi_2^j) = \sum_j b_j T_{21}^F(\phi_2^j).$$

But  $T_{21}^F(\phi_2^j) = \sum_i c_{ij} \phi_1^i$  for some  $c_{ij} \in \mathbb{R}$ , thus

$$T_{21}^F(g) = \sum_j b_j T_{21}^F(\phi_2^j) = \sum_j \sum_i b_j c_{ij} \phi_1^i$$

where  $T_{21}^F(g) = f = \sum_i a_i \phi_1^i$ . Therefore, the functional map  $T_{21}^F$  can be encoded as a compact matrix  $C_{21} = [c_{ij}]_{i,j=0}^k$  between the coefficients.

### 1.3 NAM for any basis

In this section, we show how we can define an alternative of NAM which generalizes to the adjoint of any embeddings derived from a basis.

We first prove the following statement:

**PROPOSITION 1.3.** *Given a Functional Map  $C_{21}$  and its adjoint  $A_{12}$ ,*

$$\begin{aligned} E(\Pi_{21}, A_{12}) &= \|\Pi_{21}\Phi_2 A_{12} - \Phi_1\|_{HS} \\ &= \|\Pi_{21}\Phi_2 A_{12} \sqrt{\widetilde{M}_1^{-1}} - \Phi_1 \sqrt{\widetilde{M}_1^{-1}}\| = E_{el}(\Pi_{21}, A_{12}) \end{aligned} \quad (2)$$

**PROOF.** Minimizing  $\|\Pi_{21}\Phi_2 A_{12} - \Phi_1\|_{HS}^2$  has been proven to be equal to minimizing  $\|(\sqrt{\widetilde{M}_1} \Phi_1^\dagger M_1^{-1})^\top - (\sqrt{\widetilde{M}_1} C_{21} \Phi_2^\dagger M_2^{-1})^\top\|^2$ , [Hartwig et al. 2023]. Since  $\Phi_i^\dagger = \widetilde{M}_i^{-1} \Phi_i^\top M_i$ , then  $(\sqrt{\widetilde{M}_1} \Phi_1^\dagger M_1^{-1})^\top = \sqrt{\widetilde{M}_1^{-1}} \Phi_1$ . At the same time  $(\sqrt{\widetilde{M}_1} C_{21} \Phi_2^\dagger M_2^{-1})^\top = \Phi_2 \widetilde{M}_2^{-1} C_{21}^\top \sqrt{\widetilde{M}_1}$  this means

that we are looking for embeddings similar in  $\Pi_{21}\Phi_2\tilde{M}_2^{-1}C_{21}^T\sqrt{\tilde{M}_1} \approx \Phi_1\tilde{M}_1^{-1}\sqrt{\tilde{M}_1}$ . But  $A_{12} = \tilde{M}_2^{-1}C_{21}^T\tilde{M}_1$  and so minimizing

$$E_{el}(\Pi_{21}, A_{12}) = \|\Pi_{21}\Phi_2A_{12}\sqrt{\tilde{M}_1}^{-1} - \Phi_1\sqrt{\tilde{M}_1}^{-1}\| \quad (3)$$

is equal to minimizing the initial equation. So we have the thesis.  $\square$

This means that, for any basis, the Equation (3.8) is minimized by (3.9). This energy is the generalization of energy (3.4).

This means that if a NAM with LBO is defined as the solution of  $E_{NAM}(h) = \|\Pi_{21}h(\Phi_2^k) - \Phi_1^k\|$  its generalized version is the one which minimizes

$$E_{NAM}^{new}(h) = \|\Pi_{21}h(\Phi_2^k)\sqrt{\tilde{M}_1}^{-1} - \Phi_1^k\sqrt{\tilde{M}_1}^{-1}\| \quad (4)$$

On the other hand, given a NAM  $h$ , we can convert to a  $\Pi_{21}$  performing

$$T_{21} = NS(\Phi_1^k\sqrt{\tilde{M}_1}^{-1}, h(\Phi_2^k)\sqrt{\tilde{M}_1}^{-1}) \quad (5)$$

This is a generalized definition of NAM that includes an adjoint of other bases. However, from the practical point of view,  $\sqrt{\tilde{M}_1}^{-1}$  is not well defined for any embedding, since  $\tilde{M}_1$  is positive definite iff  $\Phi_1$  is a basis.

#### 1.4 Neural Deformations Field

Given  $\mathcal{X}_1, \mathcal{X}_2$ , a deformation field between them is defined as a diffeomorphism  $F : \mathbb{R}^3 \rightarrow \mathbb{R}^3$  such that  $F(\mathcal{X}_1) = \mathcal{X}_2$ .  $F$  has the general form of  $F(x) = xR + v(x)$ ,  $\forall x \in \mathcal{X}_1$ , where  $R \in \mathbb{R}^{3 \times 3}$  is a global affine transformation and  $v(x)$  is a generic function from  $\mathbb{R}^3$  to  $\mathbb{R}^3$ . If the shapes are rigidly alignable, then  $v(x) = t \in \mathbb{R}^1$  does not depend on  $x$ . If the shapes undergo non-rigid deformations,  $v$  is a non-linear displacement defined  $\forall x \in \mathcal{X}_1$ . A deformation field can be seen as a function that aligns the point of deformable shapes. Recent works, inspired by *Neural fields*, parameterize this deformation through a multilayer perception  $\bar{F}$ , namely the neural deformation field [Attaiki and Ovsjanikov 2024; Li 2022; Li et al. 2021; Park et al. 2021; Tang et al. 2023]. Given a correspondence  $\Pi_{21}$  this neural deformation field  $\bar{F}$  can be estimated by minimizing

$$E(\bar{F}) = \|\bar{F}(X_1) - \Pi_{21}X_2\|, \quad (6)$$

where  $X_1$  and  $X_2$  are sampling on the shapes and  $\|\cdot\|$  is the Frobenius norm. With our work, we bring this concept to functional domains, modeling a neural representation to align any pair of embeddings.

#### 1.5 Role of Non linearity

In this section, we give a quantitative evaluation of our theoretical motivation of Section 4.2 of the main paper.

In Figure 1, we show the effect of NAM representation in terms of the alignment of embeddings and of the quality of the converted map.

We define the spectral discrepancy between two truncated basis  $\Phi_1^k, \Phi_2^k$ , with  $k \leq 200$  as

$$SD(\Phi_1^k, \Phi_2^k) = \sum_{j=0}^k ((\Phi_2^{200})^\dagger \psi^j - (\Phi_1^{200})^\dagger \Gamma_{12} \phi_1^j)^2 \quad (7)$$

where  $\Psi^k = \Phi_2^k A_{12}$  in the linear case and  $\Psi^k = h(\Phi_2^k)$  for NAM.

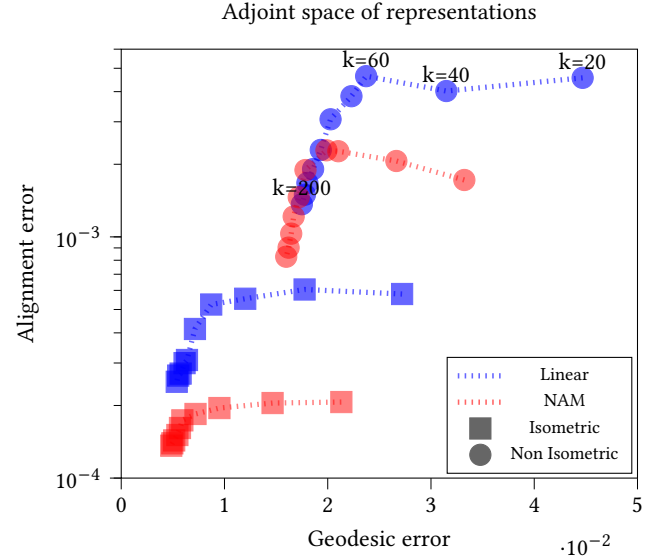


Fig. 1. Results of linear alignment vs NAM. On the  $x$ -axis the geodesic error of the recovered map. On the  $y$ -axis the alignment error is computed as the Euclidean distance between the embeddings. The introduction of the non-linear module induces a better alignment of the basis and consequently a better correspondence estimation. We note that as we increase the basis dimension (from right to left), the difference between the NAM representation and the linear one decreases.

In Figure 2, we depict the difference between the frequencies of two truncated embeddings. The basis functions of the source basis present also high dimensional frequencies of the basis of the target. We report also a metric on all the shapes of two dataset quantifying this frequency difference between the spectrum. As expected, in the non-isometric case this value is larger than in the isometric case.

In Table 1, we report the Mean Spectral Discrepancy for different datasets. We note that the more isometric the dataset, the lower the discrepancy metric for the linear case.

	DT4D intra	SHREC19	SMAL	DT4D inter
Linear	2.89 e-07	9.87e-07	1.45e-06	8.35 e-07
NAM	3.2e-08	1.55e-07	4.25e-07	1.14e-07

Table 1. Mean spectral discrepancy on different datasets. We can see that in the isometric case, the spectral discrepancy of the Linear map is lower than in the other cases.

#### 1.6 Kinect Dataset

In this section, we add details on how we built our evaluations on point clouds. We considered the [Bhatnagar et al. 2022] dataset of Kinect acquisitions of humans interacting with objects. We selected 15 shapes. Then we randomly selected 10k points from each shape. Having the SMPL registration, for each point of the SMPL dataset, we extracted outliers considering the points with a distance with the SMPL surface below a threshold.

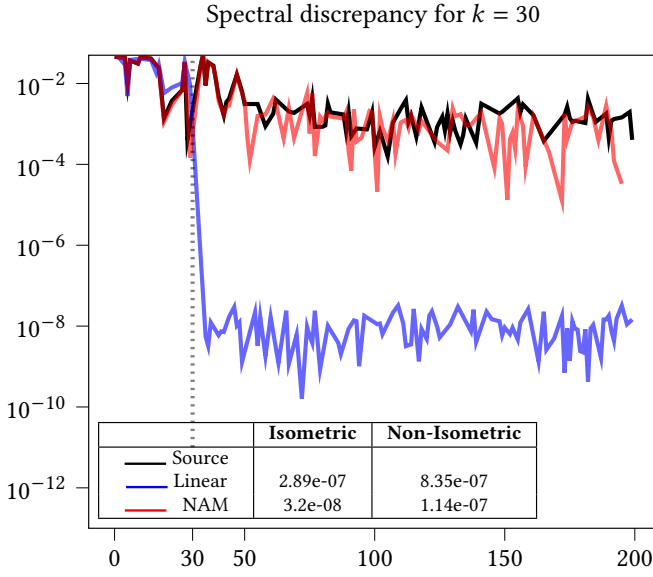


Fig. 2. We consider  $\sum_{j=0}^{30} ((\Phi_2^{200})^\dagger \psi^j)^2$ , where  $\psi^j$  is  $\Pi_{12}\phi_1^j$  for Source,  $h(\Phi_2)|_j$  for NAM and  $(\Phi_2 A_{12})|_j$  for linear, where  $\cdot|_j$  is the  $j^{th}$  column. We note that  $\Pi_{12}\phi_1^j$  on average on  $j$  has small components in all the frequency bandwidth of  $\Phi_2^{200}$ . Similar behaviour is obtained by NAM while the linear alternative is similar only on the first frequencies. In the table, we compute the Mean Spectral Discrepancy for Linear and NAM representation for each couple of the dataset as  $MSD(\Phi_1, \Phi_2) = \sum_{k=0}^K SD(\Phi_1^k, \Phi_2^k)$ . We can see that the more non-isometric the dataset, the bigger the MSD with the Linear map.

In figure 3 we show the 15 shapes that our evaluation dataset comprises.

### 1.7 Additional Results

In the following table, we report the values of ZO, NZO, and NZO\* with different  $k_{ini}$ . This highlights that if the initial map is too good we can increase its accuracy only if we find an initial number of  $k$  enough to represent completely the correspondence. Instead, in more challenging scenarios as in the SMAL dataset, converting to a lower dimensional map can help decrease the error because it induces more smoothness.

	DT4D intra		SMAL	
	$k_{ini} = 20$	$k_{ini} = 100$	$k_{ini} = 20$	$k_{ini} = 100$
Ini	0.90	0.90	7.10	7.10
ULRSM ref	0.85	0.85	3.87	3.87
ZO	1.06	0.84	6.02	6.78
NZO	0.99	0.84	4.39	4.89
NZO*	1.9	1.7	3.97	3.86

Table 2. NZO performances for different initial basis dimensions

Depth	Width 64			Width 128			Width 256		
	Gt	Est.	Time	Gt	Est.	Time	Gt	Est.	Time
1	0.94	<b>0.61</b>	<b>2.3</b>	0.89	<b>0.61</b>	2.4	0.86	0.62	<b>2.3</b>
2	0.86	<b>0.61</b>	2.6	<b>0.84</b>	0.63	2.6	<b>0.84</b>	0.65	2.6
4	<b>0.84</b>	0.63	3.0	0.87	0.65	2.9	0.87	0.68	2.8
8	0.89	0.66	3.5	0.90	0.64	3.4	0.95	0.64	4.3

Table 3. Ablation study on Width and Depth.

### 1.8 Ablation

*Number of parameters.* A feature on which we ablate is the number of parameters of our model, i.e. the depth and the width of the non-linear component. In Table 3 we report the mean geodesic errors obtained by choosing different values of depth and width. Interestingly, comparing mean optimization time and refinement performances, the optimal number is 2 layers. For the width, we have different behaviors. If the initial map is estimated by a learned feature extractor, the best choice is a width of 64. However, in the case of a better map computed from a ground-truth functional map, the best choice seems to be the more expensive. For this reason, we decided to make a conservative choice, which returns intermediate results. In general, as the number of parameters and non-linearities increases, the solution space expands, making optimization more expensive and solutions less smooth and so less accurate.

*Alternatives.* We add details on the alternatives to which we compare our NAM approach in the ablation. Some alternatives to induce bijectivity are:

- (A) Overfit a correspondence with a Neural deformation field.
- (B) Optimize two networks that represent two deformation fields,  $f, g$ , and impose a bijectivity loss explicitly

$$\mathcal{L}_{cycle} = \|g(f(V_1)) - V_1\| + \|f(g(V_2)) - V_2\| \quad (8)$$

---

#### ALGORITHM 1: ZoomOut

---

- 1: Input:  $\Pi_{21}$
  - 2: **for**  $k_{ini} \leq k \leq k_{end}$  **do**
  - 3: Optimize for a Functional map  $C_{21}^k$  minimizing Equation
$$\|\phi_1^k C_{21}^k - \Pi_{21} \phi_1^k\|$$
  - 4: Compute  $\Pi_{21} = NS(\Phi_1^k, \Phi_2^k C_{21}^k)$
  - 5: **end for**
  - 6: Output:  $\Pi_{21}$
- 

---

#### ALGORITHM 2: NeuralZoomOut

---

- 1: Input:  $\Pi_{21}$
  - 2: **for**  $k_{ini} \leq k \leq k_{end}$  **do**
  - 3: Optimize for a NAM  $h$  minimizing Equation
$$\|\Pi_{21} h(\phi_2^k) - \phi_1^k\|$$
  - 4: Compute  $\Pi_{21} = NS(\Phi_1^k, h(\Phi_2^k))$
  - 5: **end for**
  - 6: Output:  $\Pi_{21}$
-

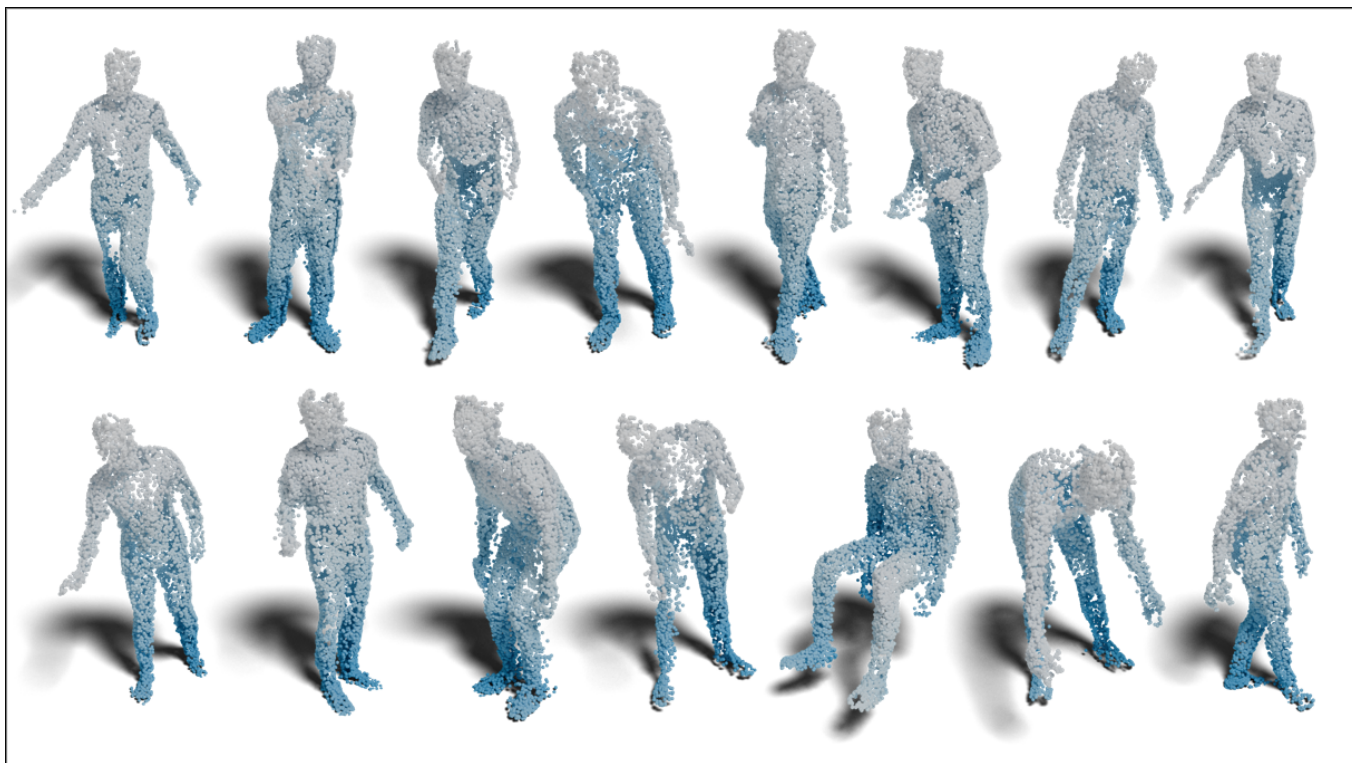


Fig. 3. The Kinect Test Dataset: the 15 selected shapes of the Kinect dataset used for evaluation

## References

- Souhaib Attaiki and Maks Ovsjanikov. 2024. Shape Non-rigid Kinematics (SNK): A Zero-Shot Method for Non-Rigid Shape Matching via Unsupervised Functional Map Regularized Reconstruction. arXiv:2403.06804 [cs.CV]
- Bharat Lal Bhatnagar, Xianghui Xie, Ilya A. Petrov, Cristian Sminchisescu, Christian Theobalt, and Gerard Pons-Moll. 2022. BEHAVE: Dataset and Method for Tracking Human Object Interactions. arXiv:2204.06950 [cs.CV] <https://arxiv.org/abs/2204.06950>
- Florine Hartwig, Josua Sassen, Omri Azencot, Martin Rumpf, and Mirela Ben-Chen. 2023. An Elastic Basis for Spectral Shape Correspondence. In *ACM SIGGRAPH 2023 Conference Proceedings* (Los Angeles, CA, USA) (*SIGGRAPH '23*). Association for Computing Machinery, New York, NY, USA, Article 58, 11 pages. doi:10.1145/3588432.3591518
- Tatsuya Harada Li, Yang. 2022. Non-rigid Point Cloud Registration with Neural Deformation Pyramid. arXiv:2205.12796
- Xueqian Li, Jhony Kaesemodel Pontes, and Simon Lucey. 2021. Neural Scene Flow Prior. arXiv:2111.01253 [cs.CV] <https://arxiv.org/abs/2111.01253>
- Keunhong Park, Utkarsh Sinha, Jonathan T. Barron, Sofien Bouaziz, Dan B Goldman, Steven M. Seitz, and Ricardo Martin-Brualla. 2021. Nerfies: Deformable Neural Radiance Fields. *ICCV* (2021).
- Jiapeng Tang, Lev Markhasin, Bi Wang, Justus Thies, and Matthias Nießner. 2023. Neural Shape Deformation Priors. arXiv:2210.05616 [cs.CV] <https://arxiv.org/abs/2210.05616>